

DEFT: Distilling Entangled Factors

Jiantao Wu¹ Lin Wang¹ Chunxiuzi Liu¹ Fanqi Li¹

Abstract

Disentanglement is a highly desirable property of representation due to its similarity with human understanding and reasoning. However, the performance of current disentanglement approaches is still unreliable and largely depends on the hyperparameter selection. Inspired by fractional distillation in chemistry, we propose DEFT, a disentanglement framework, to raise the lower limit of disentanglement approaches based on variational autoencoder. It applies a multi-stage training strategy, including multi-group encoders with different learning rates and piecewise disentanglement pressure, to stage by stage distill entangled factors. Furthermore, we provide insight into identifying the hyperparameters according to the information thresholds. We evaluate DEFT on three variants of dSprites and SmallNORB, showing robust and high-level disentanglement scores.

1. Introduction

The basis of artificial intelligence is to understand and reason about the world based on a limited set of observations. Unsupervised disentanglement learning is highly desirable due to its similarity with the way humans think. For instance, we can infer the movement of a running ball based on a single glance. The human brain is capable of disentangling the positions from a set of images without supervision. It has been suggested that a disentangled representation is helpful for a large variety of downstream tasks (Schölkopf et al., 2012; Peters et al., 2017). According to Kim & Mnih (2018), a disentangled representation promotes interpretable semantic information. That brings substantial advancement, including but not limited to reducing the performance gap between humans and AI approaches (Lake et al., 2017; Higgins et al., 2018). Other instances of disentangled representation include semantic image understanding and generation

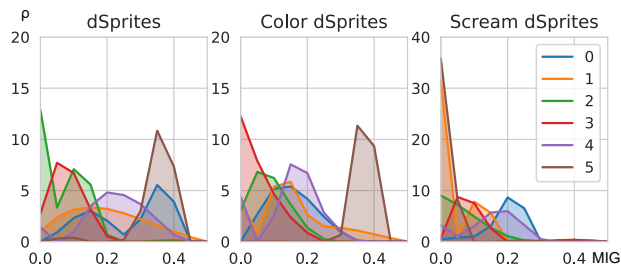


Figure 1. The distributions of MIG scores on dSprites, Color dSprites, and Scream dSprites. Models are abbreviated (0= β -VAE, 1=FactorVAE, 2=DIP-VAE-I, 3=DIP-VAE-II, 4= β -TCVAE, 5=AnnealedVAE). The scores are measured from the mean representation of 50 models with the tuned hyperparameter for best mean MIG score. See more in Sec. 4.

(Lample et al., 2017; Zhu et al., 2018; Elgammal et al., 2017), zero-shot learning (Zhu et al., 2019), and reinforcement learning (Higgins et al., 2017b).

The core of science is to find the invariant law of the world. The consequence predominated by the law should be reproducible and low variance, yet, the current disentanglement approaches showed inconsistency (Locatello et al., 2019). We analyzed 5400 models on three variants of dSprites for six disentanglement approaches and six hyperparameters¹. Fig. 1 shows the MIG distributions of six disentanglement approaches with the best hyperparameter settings, and one can see a large number of trails have low MIG scores. In other word, the results depend on luck to a certain degree. Thus, a stable and reliable approach is vital to study further and work in practice.

The information leakage indicates that one factor’s information leaks into two or more latent variables; thus, the disentanglement scores fluctuate in training. We investigate this phenomenon on dSprites using β -VAE($\beta = 6$) (see Sec. 4), and trace the MIG scores while training. We find that the information leakage happens and causes the fluctuation of MIG scores by tracing the max-2 normalized mutual information (NMI) matrix (seeing EQ. 6).

^{*}Equal contribution ¹Shandong Provincial Key Laboratory of Network Based Intelligent Computing, University of Jinan, Jinan, China. Correspondence to: Jiantao Wu <cloudcrow@gmail.com>, Lin Wang <wangplanet@gmail.com>.

¹We use the pretrained models provided by [disentanglement.lib](#).

Inspired by the fractional distillation in chemistry, we can divide the training process into several stages, and extract components as “pure” as possible in each stage. In this paper, we propose a process distilling entangled factors (DEFT) from observations to address the information leakage problem. DEFT applies different disentanglement pressure to allow partial information passing through the information bottleneck at each stage. Moreover, DEFT consists of multiple encoders with different learning rates to retain the learned codes, reducing information leakage. We also propose *anneal test* to determine the piecewise disentanglement pressures by information thresholds relative to the inductive biases on the data. Our contributions are summarized in the following:

- We propose a DEFT method to distill entangled factors stage-by-stage, in which each encoder is only responsible for learning partial information with a narrow information bottleneck at each stage.
- We propose an anneal test to determine the hyperparameters for manifesting the potential of DEFT.

2. Background

Disentanglement learning is fascinating and challenging because of its intrinsic similarity to human intelligence. As depicted in the seminal paper by Bengio et al., humans can understand and reason from a complex observation to the explanatory factors. A typical modeling assumption of disentanglement learning is that a set of independent factors generates the observed data. The task of disentangling factors of variation is to learn a representation separating the ground-truth factors into different dimensions on latent space. Current studies usually evaluate proposed approaches on the artificial datasets with label information for measuring the disentanglement score. The popular applied datasets include dSprites (Matthey et al., 2017), CelebA (Liu et al., 2015), Shapes3D (Burgess & Kim, 2018), Face3D (Heseltine et al., 2008), Cars3D (Kim & Mnih, 2018), and SmallNORB (LeCun et al., 2004). The disentanglement metric is also crucial for this domain, yet there is no widely accepted metric. The available metrics include BetaVAE metric (Higgins et al., 2017a), FactorVAE metric (Kim & Mnih, 2018), Mutual Information Gap (Chen et al., 2018), Modularity (Ridgeway & Mozer, 2018), DCI (Eastwood & Williams, 2018), SAP score (Kumar et al., 2018), UDR (Duan et al., 2020), and IIS (informativeness, interpretability, and separability) (Do & Tran, 2020).

Higgins et al. (2017a) find the KL term’s pressure in VAE encourages the disentanglement; they propose β -VAE to introduce an extra hyperparameter for better disentanglement. However, the selection of β is a trade-off between the reconstruction error and the disentanglement. Burgess

et al. (2018) propose an annealed version, AnnealedVAE, to overcome this issue and achieve low reconstruction error and high disentanglement score. They suggest that a gradually increasing information bottleneck enforces the model to utilize those extra bits for the best improvement codes. Kim & Mnih (2018); Chen et al. (2018) argue that a heavier penalty on the total correlation between the latent variables encourages the model to learn a more disentangled representation. β -TCVAE (Chen et al., 2018) decomposes the KL term into the *index-coded mutual information* (MI), the *total correlation* (TC), and the *dimension-wise KL* (DWKL). FactorVAE (Kim & Mnih, 2018) estimates the TC term by a multi-layer perceptron. Other approaches like DIPVAE (Kumar et al., 2018) can also enforce the aggregate posterior of the latent to be statistically independent. These approaches avoid diminishing the mutual information between the observations and the latent variables, achieving both a high disentanglement score and a low reconstruction error.

Though promoting independence obtains the SOTA performance on these artificial datasets, the fundamentals are doubted by Locatello et al. (2019). They claimed, “We do not find any evidence that they can be used to reliably learn disentangled representations in an unsupervised manner as hyper parameters seem to matter more than the model and good hyperparameters seemingly cannot be identified without access to ground-truth labels.”

3. Preliminary

3.1. Disentanglement Approaches

VAE The variational autoencoder (Kingma & Welling, 2013) is a popular generative model, assuming that the latent variables obey a specific prior (normal distribution in practice). The key idea of VAE is maximizing the likelihood objective by the following approximation:

$$\mathcal{L}(\theta, \phi; x, z) = \mathbb{E}_{q_\phi(z|x)} [\log p_\theta(x|z)] - D_{\text{KL}}(q_\phi(z|x) || p(z)). \quad (1)$$

β -VAE Higgins et al. (2017a) discovered the relationship between the disentanglement and the KL divergence penalty strength. They propose the β -VAE maximizing the following expression:

$$\mathcal{L}^1(\theta, \phi; x, z; \beta) = \mathbb{E}_{q_\phi(z|x)} [\log p_\theta(x|z)] - \beta D_{\text{KL}}(q_\phi(z|x) || p(z)). \quad (2)$$

β controls the pressure for the posterior $Q_\phi(z|x)$ to match the factorized unit Gaussian prior $p(z)$. However, there is a trade-off between the quality of reconstructed images and the disentanglement. A high value of β leads to a lower implicit capacity of the latent information and ambiguous reconstructions but a high disentanglement score.

AnnealedVAE Burgess et al. (2018) proposed the AnnealedVAE that progressively increases the information capacity of the latent variables while training:

$$\mathcal{L}^2(\theta, \phi; x, z, C) = \mathbb{E}_{q_\phi(\mathbf{z}|\mathbf{x})} [\log p_\theta(x|z)] - \gamma |D_{\text{KL}}(q_\phi(z|x)||p(z)) - C|, \quad (3)$$

where γ is a large enough constant to constrain the latent information, C is a value gradually increased from zero to a large number to produce high reconstruction quality.

β -TCVAE One popular disentangled prior assumes that the factors on the observations are independent. A series of methods enforce the independence between the latent variables, avoiding diminishing the reconstruction error. FactorVAE (Kim & Mnih, 2018) applies a discriminator to calculate the total correlation (TC, (Watanabe, 1960)) approximately; β -TCVAE (Chen et al., 2018) promotes the TC penalty by decomposing the KL term; DIP-VAE (Kumar et al., 2018) identifies the covariance matrix of $q(z)$. Here, we chose β -TCVAE as the representatives of these approaches. The objective of β -TCVAE is

$$\begin{aligned} \mathcal{L}^3(\theta, \phi; x, z; \beta) = & \mathbb{E}_{q_\phi(\mathbf{z}|\mathbf{x})} [\log p_\theta(x|z)] \\ & - \mathbb{E}_{q(z,n)} \left[\log \frac{q_\phi(z|n)p(n)}{q_\phi(z)p(n)} \right] \\ & - \beta \mathbb{E}_{q_\phi(z)} \left[\log \frac{q_\phi(z)}{\prod_j q_\phi(z_j)} \right] \\ & - \sum_j \mathbb{E}_{q_\phi(z_j)} \left[\log \frac{q_\phi(z_j)}{p(z_j)} \right]. \end{aligned} \quad (4)$$

3.2. Disentanglement Metrics

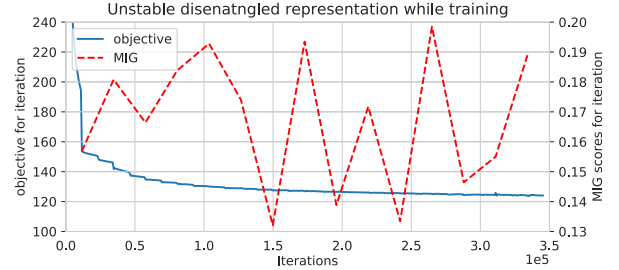
The notion of disentanglement is still an open topic, and there does not exist a widely accepted definition. Therefore, one metric is hard to assess disentanglement, and there are four metrics applied in this paper: DCI, MIG, Modularity, DCI. Among them, MIG detects axis-alignment, is unbiased and suitable to any latent distributions.

The mutual information measures an information-theoretic quantity between a latent z_j and a factor v_k . we define the m th largest normalized mutual information (NMI) between z_j and v_k as max- m NMI(v_k):

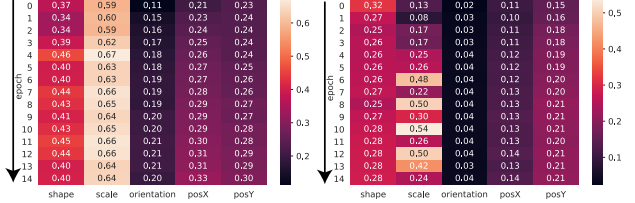
$$\text{max-}m \text{ NMI}(v_k) = \max_j \frac{1}{H(v_k)} I_n(z_j; v_k), \quad (5)$$

where \max_j^m returns the m th largest element among index j . The calculation of MIG can be written as:

$$\frac{1}{K} \sum_{k=1}^K \text{max-1 NMI}(v_k) - \text{max-2 NMI}(v_k). \quad (6)$$



(a) disentangled score fluctuation



(b) max-1 NMI

(c) max-2 NMI

Figure 2. Failure pattern on dSprites. (a) The curves of the objective and MIG score. (b) max-1 NMI(v_k) over training. (c) max-2 NMI(v_k) over training. Each row in (b) and (c) corresponds to the NMI vector of factors at an epoch. Please notice that, despite the smooth trend shown in disentangling primary mutual information (b), the process for secondary mutual information is not that stable, especially for the scale factor (c).

4. Unstability of disentanglement approaches

We observe a high variance of disentanglement from the comprehensive study of disentanglement approaches (Locatello et al., 2019). It implies these models are unreliable, and there exists a failure pattern that violates disentanglement. A perfect disentangled representation should project the factors into one latent variable. Therefore, it has high values of the max-1 NMI vector max-1 NMI(v_k) and low values of the max-2 NMI vector max-2 NMI(v_k). In other words, the learned representation re-entangles when the max-1 NMI decreases or the max-2 NMI increases.

We conducted experiments on dSprites with the standard β -VAE ($\beta = 6$). We traced the normalized mutual information between the observations and the latent variables at each epoch's end. The MIG scores fluctuated while training, as depicted in Fig. 2a. Fig. 2bc shown the changes in NMI over training. One can see that the fluctuating values of max-2 NMI vector were the main obstacle to disentangle factors. The increase of max-2 NMI indicated two or more latent variables learned information from one factor (scale). We also noticed this phenomenon happen on the other datasets or by the other disentanglement approaches. Thus, preventing information leakage could improve disentanglement significantly.

5. DEFT

5.1. Information Threshold

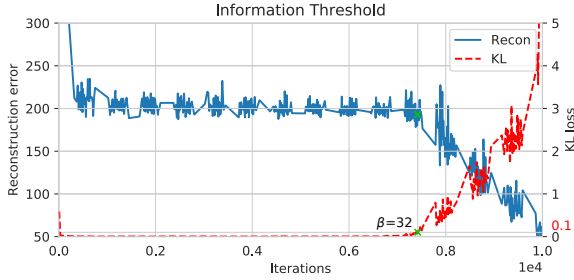


Figure 3. Information threshold. The model starts to learn information at iteration 7500 ($\beta = 32$), where KL raising and reconstruction error reducing.

Burgess et al. (2018) suggests the close relationship between the information bottleneck principle and β in β -VAE. Though high disentanglement pressure encourages disentanglement, an over-high value of β leads to the latent variables share no information between the observations. We can infer there is a critical point of β so that the model starts to learn information from the observations, and we call this point *information threshold*. Therefore, we introduce the *anneal test* to determine the threshold for a given dataset. The objective is the same as β -VAE, but uses an annealed β from a high value to one. (which starts with a very high value and ends with value 1) As the KL term’s pressure decaying, there exists a critical point that the model learns information from the dataset when decaying the reconstruction error and raising the KL loss. For example, we train the model with an annealed β from 200 to 0 in 100000 iterations. As shown in Fig. 3, the threshold is approximately 52 at iteration 7400. Roughly, we regard the model learns information when the KL loss raises over 0.1.

5.2. Proposed Framework

To overcome information leakage, the main difficulty is retaining disentangling in previously learned factors. We propose a framework to *distill entangled factors (DEFT)* from the observations like the process of *fractional distillation in chemistry*. This framework provides deft settings to distill factors of variation and guarantees the improvement of disentanglement in each stage. It has multiple encoders with different learning rates and uses piecewise disentanglement pressures. The decoder of DEFT takes the concatenated latent from the outputs of these encoders. In each training stage, only one active encoder has a primary learning rate lr_1 , and the other inactive encoders have a secondary learning rate $\gamma \times \text{lr}_1$ ($0 \leq \gamma \leq 1$). DEFT pushes a disentanglement pressure following a piecewise constant

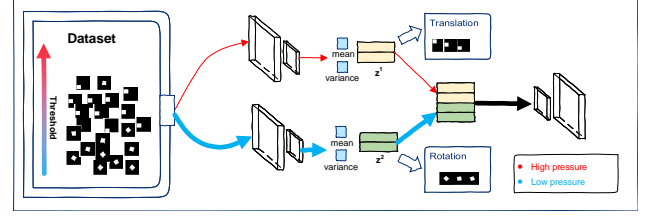


Figure 4. Architecture of DEFT. The information thresholds on the toy dataset vary from blue to red. In the first stage, the first encoder extracts translation with high pressure by blocking information of rotation. In the second stage, the second encoder extracts the residual component by extending the information bottleneck.

decay schedule to impose the different factors emerging in each stage. Furthermore, DEFT is capable of the disentanglement approaches based on variational autoencoder, and we chose β -VAEs as the base method in the main part of this paper.

The architecture of DEFT is shown in Fig. 4. There are two independent groups of encoders receiving the input images. Then, the concatenated latent variables are fed the outputs of these encoders into the decoder. DEFT learns disentangled factors in the corresponding stages.

Algorithm 1 The algorithm of DEFT.

Input: pressure β_j , stages m
Initialize $\theta, \{\phi_i\}$ for $p_\theta(x|z), \{q_{\phi_i}^i(z|x)\}$.
for $j = 0$ **to** $m - 1$ **do**
 $x = \text{sample}()$
 $z = \text{concat}(\{\text{reparameterize}(q_{\phi_i}^i(x))\})$
 $g_\theta, \{g_{\phi_i}\} = \nabla_{\theta, \{\phi_i\}} \mathcal{L}(\theta, \{\phi_i\}; x, z; \beta_j)$
for $i = 0$ **to** $m - 1$ **do**
if $i = j$ **then**
 $\phi_i = \phi_i - g_{\phi_i} \times \text{lr}_1$
else
 $\phi_i = \phi_i - g_{\phi_i} \times \text{lr}_1 \times \gamma$
end if
end for
 $\theta = \theta - g_\theta \times \text{lr}_1$
end for

6. Experiment

Settings We refer to the experiment settings in (Higgins et al., 2017a). There are two types of encoder architecture and one decoder architecture in this paper. The encoder consists of 4 convolutional layers for the standard settings, each with 32 channels, 4x4 kernels, and a stride of 2. Then, the outputs of the encoder are fed into one fully connected layer of 256 units. After that, one fully connected layer of 20 units parameterized the mean and log standard deviation

of the latent distribution with 10 Gaussian random variables. For the DEFT setting, the number of channels and latent variable size is divided by the total number of groups. The decoder is almost symmetric with the encoder but applies a parameterized Bernoulli distributions over the outputs' pixels. All layers are activated by ReLU. The optimizer is Adam, with a learning rate of $5e-4$.

6.1. Hyperparameter Selection

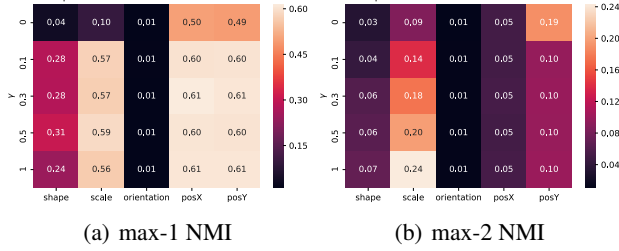


Figure 5. The max-1 and max-2 NMI vectors for γ . Columns show the mutual information of five factors. Rows show the results of independent trails with different γ .

Coefficient of secondary lr We investigated the effects of γ . The settings of DEFT were two encoders, β -VAE for the base model, and piecewise pressure with 70,30. We first trained the model on the first stage normally, then compared the normalized mutual information for different γ setting. One can see that the max-1 normalized mutual information changes slightly for those $\gamma > 0.1$, and the max-2 normalized mutual information increases as γ getting bigger except $\gamma = 0$. The experimental results indicate a small value of γ can prevent one factor's information from leaking into another dimension. However, it also violates the model to modify the learned dimension causing lower max-1 mutual information when γ is too small. In practice, $\gamma = 0.1$ keeps a good balance between increasing max-1 mutual information and decreasing max-2 mutual information.

Piecewise pressures The ideal situation is to find a set of β s to isolate information into several areas, and each area contains only "pure" information for one factor. In this paper, we do not intend to uncover the mechanism of the information threshold. We only explore it as a tool for selecting suitable hyperparameters of DEFT and prove the efficiency of DEFT. To get the distribution of the information thresholds with respect to factor c_i , we randomly sample one observation and get all samples with the same factors except factor c_i ; then, calculate the information threshold of this sub dataset by the algorithm introduced in Sec. 5.1; last, repeat the above procedures 50 times to generate enough data points.

We measured the information thresholds of factors on four

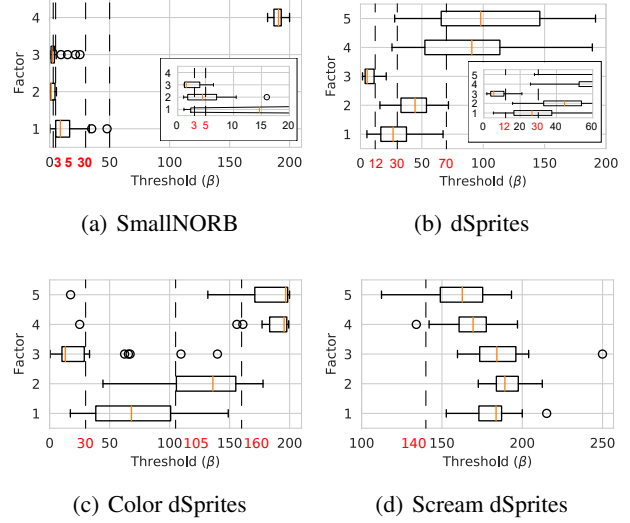


Figure 6. Information thresholds of factors on four datasets. The red number denotes the pressure to separate these factors with different information thresholds.

Table 1. Experimental settings for DEFT. γ is always 0.1.

	GROUP	EPOCHS	PRESSURES
DSPRITES	4	2,2,4,15	70,30,12,1
COLOR	4	2,2,4,15	160,105,30,1
SCREAM	2	4,15	140,1
SMALLNORB	4	20,40,40,400	30,5,3,1

datasets, as shown in Fig. 6. One can see that the normal dSprites and Color dSprites have more separable information thresholds than Scream dSprites and SmallNORB. Though the three variants of dSprites have the same factors, their information thresholds are different. The difference of information thresholds answers why the current disentanglement approaches fail to transfer hyperparameters across different problems. We summarize the piecewise pressure and the other training settings in Tab. 1.

6.2. Performance

We trained each model for 10 times and compared our model and the other six disentanglement approaches on dSprites, Color dSprites, Scream dSprites, and SmallNORB. As shown in Fig. 7, all the four metrics show the learned representations by DEFT have a lower variance than the others and have high-level scores. DEFT effectively raises the lower limit of β -VAE; however, DEFT can not boost the upper limit, which may be decided by the base approach. Interestingly, the Scream dSprites is the most challenging problem among the four, and the result in Fig. 6 (d) also indicates the factors are hard to separate. That implies an

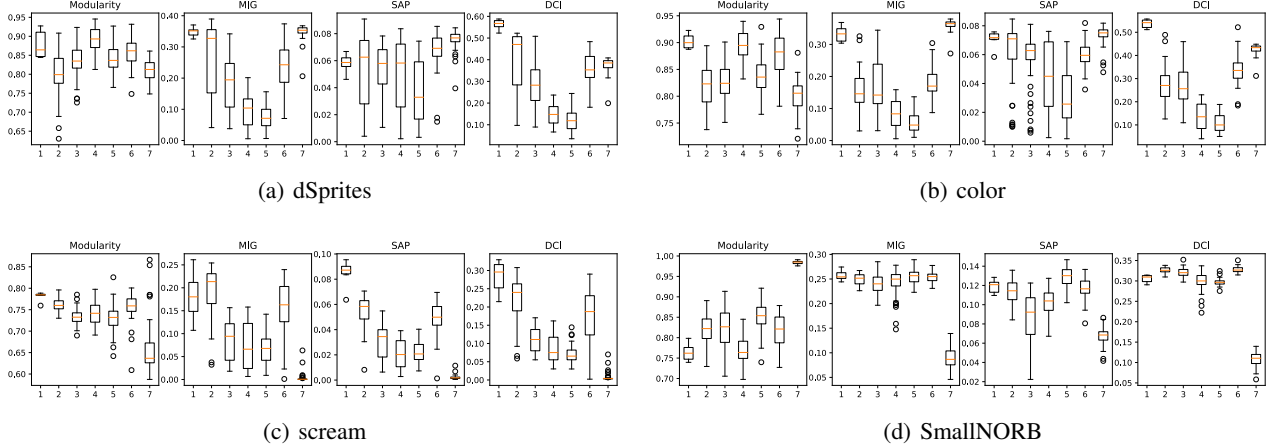


Figure 7. Disentanglement scores distribution for different approaches and datasets. Seven approaches respectively denote 1=DEFT, 2= β -VAE, 3=FactorVAE, 4=DIP-VAE-I, 5=DIP-VAE-II, 6= β -TCVAE, and 7=AnnealedVAE.

internship between disentanglement and information thresholds.

In this part, we show the changes of MIG scores in different stages in Fig. 8. All experimental results on four datasets reveal that DEFT got low scores in the first stage and gradually improved in the following stages. However, DEFT failed to raise the lower limit of disentanglement on Scream dSprites. DEFT is unable to distill entangled factors when their information thresholds are difficult to distinguish. Except that, DEFT significantly improves the lower limit of disentanglement by a multi-stage strategy.

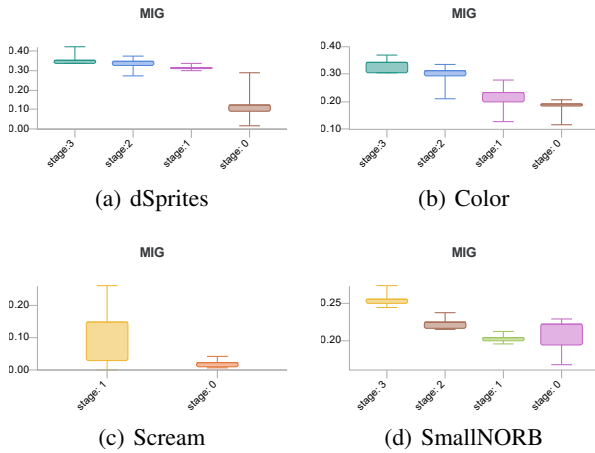


Figure 8. MIG distribution of DEFT on four datasets for different stages.

The reconstruction quality is also a desirable property. We also show the distribution of reconstruction error in Fig. 9. In general, DEFT achieves both high image quality and disentanglement.

Failure rate We regard the model fails to learn a disentangled representation if the MIG score is lower than 0.1. Tab. 2 shows the failure rates. One can see that FactorVAE and btcvae have the lowest failure rate. Though DIP-VAE encourages independence, it seems penalizing the TC term is a much more reliable method, and FactorVAE and β -TCVAE perform better than DIP-VAE. Besides, DEFT significantly decreased the failure rate comparing the other approaches.

Table 2. Failure rate (%) for each approach (column) and dataset (row).

1	2	3	4	5	6	7
8.0	47.7	11.0	76.0	87.0	18.7	61.7
0.0	36.0	16.7	78.0	89.3	23.7	47.7
12.0	34.3	66.7	80.3	89.0	43.7	100.0
0.0	0.0	0.0	28.7	0.0	0.0	88.0

6.3. Ablation Study

Normal encoder with piecewise pressures We applied experimental settings in Tab. 1 except the encoder part. We trained DEFT with a normal encoder on dSprites. Each trial repeated 10 times. From Fig. 10a, the MIG scores got the average in the first stage and diffused in the following stages.

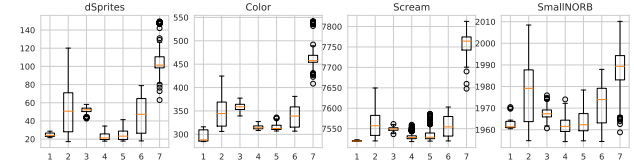


Figure 9. Distribution of reconstruction error.

We further investigated the reason and traced the normalized max-1 mutual information between the latent z_0 and the observations in Fig. 10b. Though this latent variable learned the disentangled factor (posX) in the first stage, it could not retain information when the information bottleneck was extended.

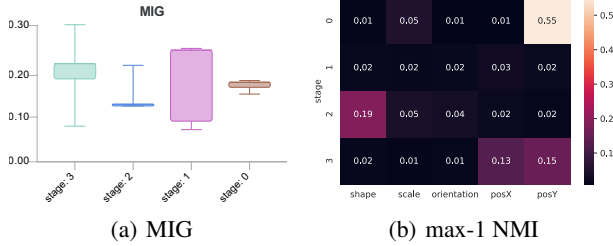


Figure 10. DEFT with a normal encoder. The distribution of MIG score for four stages (left). The max-1 NMI, $I_n(z_0; v_k)$ (right).

Multiple encoders without piecewise pressures We removed the piecewise pressures and applied a constant pressure while training. The encoder part was consist of two encoders with different learning rates (lr_1, lr_2), and the other parts were the same as β -VAE ($\beta = 6$). We repeated this model 40 times in total. Without surprise, the differentiated encoders could not automatically separate factors into different dimensions in Fig. 11. In contrast, it had lower MIG scores and . That indicates the differentiated encoders violate the model finding the optimal. These results match the results in Fig. 7. DEFT has a significant improvement on the lower limit yet insignificant improvement on the upper limit.

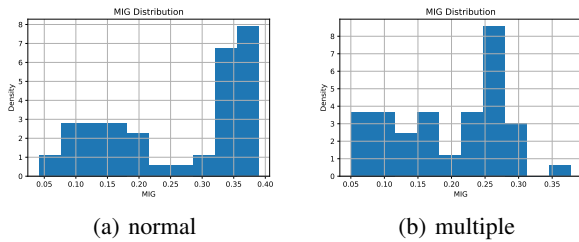


Figure 11. MIG distributions of β -VAE with a normal (a) and multiple (b) encoder(s).

6.4. Difference between AnnealedVAE

Although AnnealedVAE follows the same principles as DEFT—both use the extending information bottleneck, they focus on different properties. AnnealedVAE focuses on increasing the bottleneck; instead, DEFT focuses on retaining the learned representation. Besides, AnnealedVAE uses an increasing capacity of latent information; instead,

DEFT uses decaying pressure. The performance of DEFT seems more like β -VAE discarding the lower part see in Fig. 7. Furthermore, AnnealedVAE does not behave as they claimed. The KL term can be deposited into the MI, TC, DWKL. Our conducted experiment on dSprites showed that AnnealedVAE increased the MI term at the very beginning, and the model learned no more information after 15K iterations in Fig. 12. The increased DWKL had no help in disentanglement.

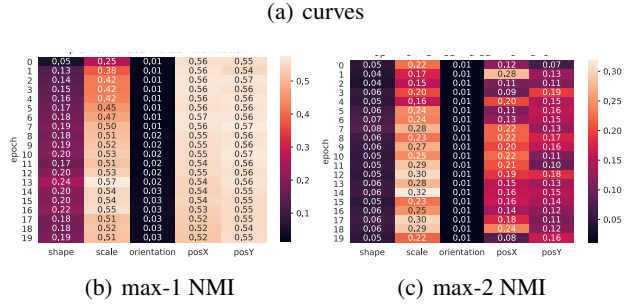
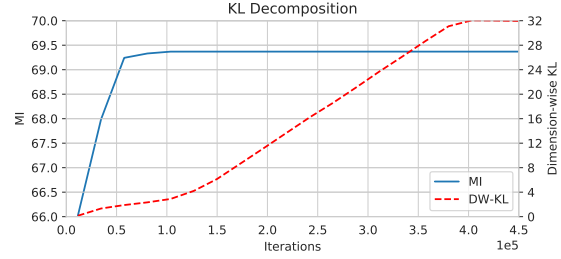


Figure 12. AnnealedVAE.

6.5. Combine with β -TCVAE

The intuitive picture we have developed of blocking partial information, enabling less factors of variation to be represented in each stage, motivated us to directly penalize the MI term in EQ. 4. The modified objective for penalizing TC is

$$\begin{aligned} \mathcal{L}^4(\theta, \phi; x, z; \alpha) = & \mathbb{E}_{q_\phi(z|x)} [\log p_\theta(x|z)] \\ & - \alpha \mathbb{E}_{q(z,n)} \left[\log \frac{q_\phi(z|n)p(n)}{q_\phi(z)p(n)} \right] \\ & - \beta \mathbb{E}_{q_\phi(z)} \left[\log \frac{q_\phi(z)}{\prod_j q_\phi(z_j)} \right] \\ & - \sum_j \mathbb{E}_{q_\phi(z_j)} \left[\log \frac{q_\phi(z_j)}{p(z_j)} \right]. \end{aligned} \quad (7)$$

We compared plain β -VAE, DEFT, and DEFT (TC) on dSprites. To be smple, we setted $\beta = 8$ for DEFT (TC). Experimental results in Fig. 13 demonstrate that both DEFT variants have rubost and high MIG scores. We had not a

comprehensive study on DEFT (TC), and DEFT is capable to other approaches.

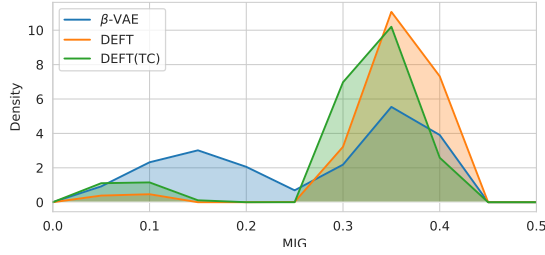


Figure 13. Distribution of MIG scores.

6.6. Model Visualization

Higgins et al. (2017a) introduced the latent traversal to visualize the generated images through the traversal of a single latent z_i . Fig. 14 shows the latent traversal of the best model with the highest MIG score. We discover some intrinsic relationship between information thresholds and disentanglement. Shape (1) and orientation (3) share the most considerable overlap of information thresholds; meanwhile, shape and orientation entangle on the same latent on dSprites. For SmallNORB, elevation and azimuth can hardly be disentangled, which have lower information thresholds. For Scream dSprites, all factors have close information thresholds, and they are also entangled in our model. For Color dSprites, posY and orientation have not been entangled.

7. Conclusion

We demonstrate the information leakage problem which causing the fluctuation of disentanglement scores. We propose a deft method, DEFT, to distill different factors in each stage by changing the capacity of the information bottleneck. Our approach significantly improves the lower limit of disentanglement and decreases the failure rate for disentanglement. We have demonstrated the insights into the explanation for the difficulty of transferring hyperparameters by information thresholds. Such insights help us to select hyperparameters when the label information is available.

Although DEFT improves robustness, the upper limit is constrained by the base method. Thus, we may improve DEFT by combining other approaches. Exploring an unsupervised algorithm for determining the information thresholds is also vital for DEFT.

References

Bengio, Y., Courville, A., and Vincent, P. Representation learning: A review and new perspectives. *IEEE Transac-*

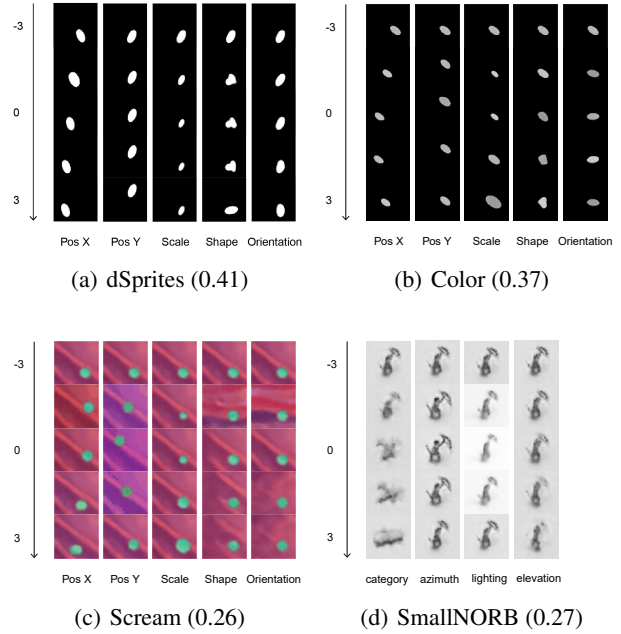


Figure 14. Latent traversal of DEFT on four datasets (MIG score). Each column shows a latent z_i and its corresponding factor (last row).

tions on Pattern Analysis and Machine Intelligence, 35 (8):1798–1828, 2013.

Burgess, C. and Kim, H. 3d shapes dataset. <https://github.com/deepmind/3dshapes-dataset/>, 2018.

Burgess, C. P., Higgins, I., Pal, A., Matthey, L., Watters, N., Desjardins, G., and Lerchner, A. Understanding disentanglement in β -vae. In *Proceedings of the 35th International Conference on Machine Learning (ICML 2018)*, 2018.

Chen, T. Q., Li, X., Grosse, R. B., and Duvenaud, D. Isolating sources of disentanglement in variational autoencoders. *arXiv preprint arXiv:1802.04942*, 2018.

Do, K. and Tran, T. Theory and evaluation metrics for learning disentangled representations. In *8th International Conference on Learning Representations (ICLR 2020)*, 2020.

Duan, S., Matthey, L., Saraiva, A., Watters, N., Burgess, C., Lerchner, A., and Higgins, I. Unsupervised model selection for variational disentangled representation learning. In *8th International Conference on Learning Representations (ICLR 2020)*, 2020.

Eastwood, C. and Williams, C. K. I. A framework for the quantitative evaluation of disentangled representations. In *6th International Conference on Learning Representations (ICLR 2018)*, 2018.

- Elgammal, A., Liu, B., Elhoseiny, M., and Mazzone, M. Can: Creative adversarial networks, generating art by learning about styles and deviating from style norms. *arXiv preprint arXiv:1706.07068*, 2017.
- Heseltine, T., Pears, N. E., and Austin, J. Three-dimensional face recognition using combinations of surface feature map subspace components. *Image and Vision Computing*, 26(3):382–396, 2008. doi: 10.1016/j.imavis.2006.12.008.
- Higgins, I., Matthey, L., Pal, A., Burgess, C., Glorot, X., Botvinick, M., Mohamed, S., and Lerchner, A. beta-vae: Learning basic visual concepts with a constrained variational framework. In *5th International Conference on Learning Representations (ICLR 2017)*, pp. 1–13, 2017a.
- Higgins, I., Pal, A., Rusu, A. A., Matthey, L., Burgess, C., Pritzel, A., Botvinick, M., Blundell, C., and Lerchner, A. DARLA: improving zero-shot transfer in reinforcement learning. In Precup, D. and Teh, Y. W. (eds.), *Proceedings of the 34th International Conference on Machine Learning (ICML 2017)*, volume 70, pp. 1480–1490, 2017b.
- Higgins, I., Sonnerat, N., Matthey, L., Pal, A., Burgess, C. P., Bosnjak, M., Shanahan, M., Botvinick, M., Hassabis, D., and Lerchner, A. SCAN: learning hierarchical compositional visual concepts. In *6th International Conference on Learning Representations (ICLR 2018)*. OpenReview.net, 2018.
- Kim, H. and Mnih, A. Disentangling by factorising. *Proceedings of the 35th International Conference on Machine Learning (ICML 2018)*, 6:4153–4171, 2018.
- Kingma, D. P. and Welling, M. Auto-encoding variational bayes. *2nd International Conference on Learning Representations (ICLR 2014)*, pp. 1–14, 2013.
- Kumar, A., Sattigeri, P., and Balakrishnan, A. Variational inference of disentangled latent concepts from unlabeled observations. *arXiv preprint arXiv:1711.00848*, 2018.
- Lake, B. M., Ullman, T. D., Tenenbaum, J. B., and Gershman, S. J. Building machines that learn and think like people. *Behavioral and brain sciences*, 40, 2017.
- Lample, G., Zeghidour, N., Usunier, N., Bordes, A., DENOYER, L., and Ranzato, M. A. Fader networks: manipulating images by sliding attributes. In I. Guyon, U. V. Luxburg, S. Bengio, H. Wallach, R. Fergus, S. Vishwanathan, and R. Garnett (eds.), *Advances in Neural Information Processing Systems (NIPS 2017)*, pp. 5967–5976. Curran Associates, Inc, 2017.
- LeCun, Y., Huang, F. J., and Bottou, L. Learning methods for generic object recognition with invariance to pose and lighting. In *Proceedings of the IEEE Computer Society Conference on Computer Vision and Pattern Recognition (CVPR 2004)*, pp. 97–104. IEEE Computer Society, 2004. doi: 10.1109/CVPR.2004.144.
- Liu, Z., Luo, P., Wang, X., and Tang, X. Deep learning face attributes in the wild. In *Proceedings of International Conference on Computer Vision (ICCV 2015)*, December 2015.
- Locatello, F., Bauer, S., Lucie, M., Rätsch, G., Gelly, S., Schölkopf, B., and Bachem, O. Challenging common assumptions in the unsupervised learning of disentangled representations. In *Proceedings of the 36th International Conference on Machine Learning (ICML 2019)*, volume 2019-June, pp. 7247–7283, 2019.
- Matthey, L., Higgins, I., Hassabis, D., and Lerchner, A. dsprites: Disentanglement testing sprites dataset. <https://github.com/deepmind/dsprites-dataset/>, 2017.
- Peters, J., Janzing, D., and Schölkopf, B. (eds.). *Elements of Causal Inference: Foundations and Learning Algorithms*. The MIT Press, 2017.
- Ridgeway, K. and Mozer, M. C. Learning deep disentangled embeddings with the f-statistic loss. In *Advances in Neural Information Processing Systems (NIPS 2018)*, volume 2018-Decem, pp. 185–194, 2018.
- Schölkopf, B., Janzing, D., Peters, J., Sgouritsa, E., Zhang, K., and Mooij, J. On causal and anticausal learning. In *Proceedings of the 29th International Conference on Machine Learning (ICML 2012)*, 2012.
- Watanabe, S. Information theoretical analysis of multivariate correlation. *IBM Journal of research and development*, 4:66–82, 1960.
- Zhu, Y., Elhoseiny, M., Liu, B., Peng, X., and Elgammal, A. A generative adversarial approach for zero-shot learning from noisy texts. In *IEEE Conference on Computer Vision and Pattern Recognition (CVPR 2018)*, pp. 1004–1013, 2018.
- Zhu, Y., Xie, J., Liu, B., and Elgammal, A. Learning feature-to-feature translator by alternating back-propagation for zero-shot learning. *arXiv preprint arXiv:1904.10056*, 2019.